(Received 19 June 2024, Accepted 30 August 2024, Scheduled 17 September 2024)

# A Symmetric Shifted Coprime Array for Localization of Mixed Near Field and Far Field Sources: Reduced Mutual Coupling Effect

Yiming Guo[3], Tao Zang[2], Fengtong Mei[1,*], Qian Liu[4], and Linzi Li[5]

[1]*Xidian University, Xi'an 710000, Shanxi, China*
[2]*Open University of Henan, Zhengzhou 450001, Henan, China*
[3]*Zhengzhou University of Industrial Technology, Zhengzhou 450001, Henan, China*
[4]*PLA Strategy Support Force Information Engineering University, Zhengzhou 450001, Henan, China*
[5]*Department of Global Cultural Integration, Kangwon National University, Chunchuan City 24205, Gangwon, Korea*

**ABSTRACT:** Sparse arrays have the technical advantages of large equivalent aperture, high degrees of freedom (DOFs), and low mutual coupling leakage. In this article, a novel symmetric sparse array, termed as symmetric shifted coprime array (SSCA), is proposed for the localization of both the far-field and near-field of sources. It can be generated in two steps. Firstly, the second subarray of the traditional coprime array is shifted by a appropriate distance, and secondly, the entire array is flipped. By translating, the proposed array provides increased DOFs and enhanced ability to resist heavy levels of mutual coupling. Meanwhile, the symmetric structure of the array can be ensured by flipping to solve the parameter estimation of mixed fields. We provide an analytical expression for the proposed array and also derive its DOFs and weight functions. The first three weight functions of SSCA are equal to 2, indicating that the SSCA improves the ability to resist mutual coupling. Numerical results show that the proposed array is superior to existing sparse arrays for both direction of arrival (DOA) and range estimations.

## 1. INTRODUCTION

Passive source location is a crucial research topic in array signal processing [1]. Over the past few decades, it has attracted considerable attention [2, 3]. If the signal is beyond the Fresnel region, its wavefront is a plane wave. On this basis, multi-signal classification (MUSIC) [4], estimation of signal parameters by rotation invariance technique (ESPRIT) [5], tensor methods have been developed. However, most of these methods are based on the far field (FF) [6]. If the signal is in the Fresnel region, its wavefront is a spherical surface wave including DOA and distance [7]. On this basis, the DOA and range parameters need to be solved synchronously. At present, a variety of near-field (NF) sources detection methods have been reported [8–12]. However, it should be pointed out that all the above algorithms rely on either NF or FF. In certain practical situations, such as using microphone array to achieve the location of the sound source, it will be affected by both NF and FF, which makes the effect of these algorithms worse. In practical application, a variety of methods have been applied to mixed source location [13–16].

In mixed-field positioning, the array used is typically a symmetrical uniform linear array (SULA). To prevent the issue of imprecise estimation, it is necessary to maintain a sensor spacing of no more than a quarter wavelength, which leads to heavy levels of mutual coupling. The performance of estimation will deteriorate. The traditional SULA is limited by the number of elements in its physical array apertures. To improve physical array apertures, the sensor number needs to be increased, which will increase the cost of the system. Compared with SULA, sparse linear arrays have larger inter-element spacing, meaning that they have larger physical array apertures and are more robust under strong mutual coupling conditions. Additionally, for sparse linear arrays with $N$ sensors, there are $\mathcal{O}(N^2)$ continuous lags in the resulting difference coarray. That is, a maximum of $N^2-1$ signals can be estimated by using $N$ physical sensors.

The earliest nonuniform linear array (NLA) is a minimum redundant array [17]. Its difference coarray has no holes and minimum redundancy, but it cannot be represented by closed expression. Its design needs to be realized through computer search, so it takes a considerable amount of computation. Different from minimum redundant array, nested array (NA) [18] and coprime array [19] have the analytical expression of the array position, so the design of arrays is easy. Compressed subarray spacing mutual prime array (CACIS) is proposed in [20]. CACIS improves DOFs and increases the array aperture. Both the nested array [18] and primitive coprime array [19] can be regarded as special forms of the CACIS. A coprime array with multi-period subarrays (CAMpS) is proposed in [21]. The DOFs of this CAMpS is similar to CACIS. To further enhance the DOFs, a general nested array (GNA) is proposed in [22], which extends the nesting idea from uniform arrays to sparse arrays such as coprime arrays, nested arrays, and minimum re-

* Corresponding author: Fengtong Mei (60111mei@sina.com).

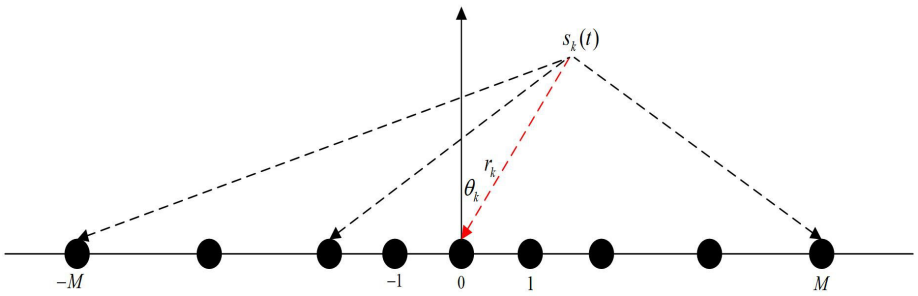


**FIGURE 1**. Source parameter diagram of mixed field sparse array.

dundant arrays. The focus of the above array design is DOFs of the array, and the influence of mutual coupling between arrays is not considered, so strong mutual coupling will lead to the degradation of DOA estimation performance. To solve this problem, a super nested array design method is proposed in [23], whose core is to extract some elements of dense subarrays in an NA array structure and scatter them into sparse subarrays. The array reduces the mutual coupling effect while maintaining the same physical aperture and freedom as the nested array. Compared with the sparse array mentioned above, it can provide a larger virtual array aperture and has a strong ability to resist mutual coupling. In [24], a thinned coprime array (TCA) is proposed by removing redundant elements from the coprime array. Under the same physical aperture and freedom conditions, the number of physical elements used by the array is smaller than that of the coprime array, which significantly reduces the mutual coupling between the elements. Ref. [25] designed a type of filling difference coarray coprime array (CAFDC). Numerical results show that the virtual array has no holes, and DOFs of the array are obviously improved. However, these arrays cannot be used directly for the estimation of mixed field parameters.

Refs. [26, 27] began to use symmetric nonuniform linear arrays (SNLAs) to locate mixed sources, and the designs of SNLAs were mainly based on nested arrays and coprime arrays. In [28], a solution to the mixed source localization problem was achieved by constructing a symmetric nested array (SNAI). Compared with the traditional SULA, the physical aperture of SNAI is larger, and the array inter-element spacing is larger. Ref. [29] proposed a symmetric double nested array (SDNA). In comparison to conventional SNAI, SNDA can generate more continuous lags and estimate more sources with physical array sensors equal in number. Ref. [30] proposed a symmetric nested array (SNAII). Compared with SNAI and SDNA, SNAII can obtain larger physical array apertures and more continuous virtual elements.

A novel array geometry, called symmetric shifted coprime array (SSCA) for the estimation of the DOA in both the FF and NF of sources, is proposed in this paper for the first time. In order to increase its DoFs and help mitigating the mutual coupling effect, we design the SSCA, which is constructed by translating and transforming on the basis of the traditional coprime array. The closed form expressions for sensor locations of the new structures are provided, along with analytical expressions for DOFs. Furthermore, the first three weight functions are derived for SSCA. Theoretical analysis shows that SSCA can effectively reduce mutual coupling while maintaining high DOFs compared to nested arrays. In strong mutual coupling scenarios, simulation results are provided to demonstrate the effectiveness and superiority of the proposed designs.

The rest of this article is organized as follows. The array signal model is introduced in Section 2. Section 3 describes the structure of the SSCA. In Section 4, the used algorithms are given. The results of the numerical simulations are presented in Section 5, and the conclusions will be drawn in Section 6.

We use the following notations throughout this paper. We use bold lowercase (uppercase) characters to represent vectors (matrices). $\odot$ represents Khatri-Rao product. vec$(\cdot)$ denotes vectorization operation. Matrix $\mathbf{C}$ is denoted using $\mathbf{C}^T$, $\mathbf{C}^H$, and $\mathbf{C}^*$ to represent its transpose, Hermitian transpose, and conjugate. The symbol $\|\cdot\|_F$ stands for a matrix's Frobenius norm. The symbol $\lfloor\cdot\rfloor$ represents a rounded-down integer. The symbol E$(\cdot)$ denotes mathematical expectation. The symbol cum$(\cdot)$ represents the fourth order cumulant. The symbol $\langle\cdot\rangle_{i,j}$ represents the number of elements in the $i$th row and $j$th column of the matrix.

## 2. PRELIMINARIES

### 2.1. Array Signal Model

Suppose that $K$ narrow band uncorrelated mixed field sources are incident on a symmetric linear array, as shown in Fig. 1, where the numbers of far-field sources and near-field sources are $K_1$ and $K_2 = K - K_1$, respectively. The coordinate set of the elements is $\mathbb{L} = [l_{-M}, \ldots, l_0, \ldots, l_M]$, where $l_i$ represents the position index of the $i$th element, $i \in [-M, M]$.

The central sensor 0 is used as the phase reference point, and the signal model received by the $i$th sensor at time $t$ is:

$$x_i(t) = \sum_{k=1}^{K} s_k(t) e^{j\tau_{ik}} + n_i(t), \tag{1}$$

where $s_k(t)$ denotes the $k$th source of information; $n_i(t)$ represents the noise of the $i$th sensor at time $t$; $\tau_{ik}$ represents the time delay between the $k$th signal incident on the $i$th sensor and the signal incident on the reference sensor. The relative propa-

gation delay of the $k$-th source received by the $i$-th sensor is

$$\tau_{ik} = \frac{2\pi r_k}{\lambda}\left(\sqrt{1+\left(\frac{id}{r_k}\right)^2 - \frac{2md\sin\theta_k}{r_k}} - 1\right), \quad (2)$$

where $\theta_k$ and $r_k$ are the DOA and distance parameters of the $k$-th signal [31]; $\lambda$ is the wavelength of the signals; $d = \lambda/4$. By expanding (2) into a second-order Taylor series, we have

$$\tau_{ik} = \left(-\frac{2\pi d}{\lambda}\sin\theta_k\right) i + \left(\frac{\pi d^2}{\lambda r_k}\cos^2\theta_k\right) i^2 + o\left(\frac{d^2}{r_k^2}\right). \quad (3)$$

According to the fresnel approximation [32], we have

$$\tau_{ik} = i\gamma_k + i^2\phi_k, \quad (4)$$

where

$$\gamma_k = -\frac{2\pi d}{\lambda}\sin\theta_k, \quad (5)$$

$$\phi_k = \frac{\pi d^2}{\lambda r_k}\cos^2\theta_k. \quad (6)$$

Therefore, using approximate relationships, the array receiving data in (1) can be simplified as

$$x_i(t) = \sum_{k=1}^{K} s_k(t) e^{j\left(i\gamma_k + i^2\phi_k\right)} + n_i(t). \quad (7)$$

Write it in matrix form [33]

$$\mathbf{x}(t) = \mathbf{A}_{\text{FF}}\mathbf{s}_{\text{FF}}(t) + \mathbf{A}_{\text{NF}}\mathbf{s}_{\text{NF}}(t) + \mathbf{n}(t), \quad (8)$$

where $\mathbf{s}_{\text{FF}}(t) = [s_1(t), \ldots, s_{K_1}(t)]^T$ and $\mathbf{s}_{\text{NF}}(t) = [s_{K_1+1}(t), \ldots, s_K(t)]^T$ denote the far-field and near-field sources vectors, respectively. $\mathbf{A}_{\text{FF}} = [\mathbf{a}(\theta_1), \ldots, \mathbf{a}(\theta_{K_1})]$ and $\mathbf{A}_{\text{NF}} = [\mathbf{a}(\theta_{K_1+1}, r_{K_1+1}), \ldots, \mathbf{a}(\theta_K, r_K)]$ denote the far-field and near-field array manifold matrices, respectively. $\mathbf{a}(\theta_k)$ and $\mathbf{a}(\theta_k, r_k)$ represent the far-field sources guidance vector and near-field sources guidance vector, respectively. The specific form is as follows

$$\mathbf{a}(\theta_k) = \left[e^{-jM\gamma_k}, \ldots, 1, \ldots, e^{jM\gamma_k}\right]^T, \quad (9)$$

$$\mathbf{a}(\theta_k, r_k) = \left[e^{j(-M\gamma_k + (-M)^2\phi_k)}, \ldots, 1, \ldots, e^{j(M\gamma_k + M^2\phi_k)}\right]^T. \quad (10)$$

According to (10), the FF signal model is a special case of the NF signal model. When $\phi_k$ is equivalent to 0, Equation (10) is reduced to (9).

### 2.2. Fourth-Order Cumulants and Difference Co-Array

In the field of array signal processing, fourth-order cumulants are commonly used. The advantage of the fourth-order statistics method is that the fourth-order statistics do not need to consider the higher-order statistics of Gaussian noise, and applying fourth-order cumulants to array signal processing can achieve array expansion, increase virtual array elements, expand array aperture, resulting in improved estimation performance. According to [29], the fourth-order cumulant output of the array is

$$\text{cum}\left\{x_m(t), x_n^*(t), x_\rho^*(t), x_q(t)\right\} = \sum_{k=1}^{K} c_{4,s_k} e^{j\left\{[(l_m - l_n) - (l_\rho - l_q)]\gamma_k + \left[\left(l_m^2 - l_n^2\right) - \left(l_\rho^2 - l_q^2\right)\right]\phi_k\right\}}, \quad (11)$$

where $x_m(t)$, $x_n(t)$, $x_\rho(t)$, and $x_q(t)$ represent the received data of the $m, n, \rho, q$-th elements at time $t$; $c_{4,s_k} = \text{cum}\{s_k(t), s_k^*(t), s_k^*(t), s_k(t)\}$ is the kurtosis of the $k$th source; $\gamma_k$ only contains the angle $\theta_k$ parameter; and $\phi_k$ contains both the angle $\theta_k$ and distance $r_k$ parameters.

In order to effectively decouple angle and distance parameters while avoiding parameter estimation failures, according to literature [28, 30], it can be concluded that by substituting $n = -m$, $q = -\rho$, into (11)

$$\text{cum}\left\{x_m(t), x_{-m}^*(t), x_\rho^*(t), x_{-\rho}(t)\right\} = \sum_{k=1}^{K} c_{4,s_k} e^{j2(l_m - l_\rho)\gamma_k}, \quad (12)$$

which can be seen as the cross-correlation between the outputs of the $m$th and $\rho$th elements of a virtual array. If $\bar{m} = m + M + 1$, $\bar{\rho} = \rho + M + 1$, $\bar{m}, \bar{\rho} \in [1, 2M+1]$ define a matrix $\mathbf{C}_1$ with a $(2M+1) \times (2M+1)$ dimension, then the elements in the $\bar{m}$th row and $\bar{n}$th column of matrix $\mathbf{C}_1$ are

$$\langle \mathbf{C}_1 \rangle_{\bar{m},\bar{n}} = \sum_{k=1}^{K} c_{4,s_k} e^{j2(l_m - l_\rho)\gamma_k}. \quad (13)$$

The matrix form of (13) is

$$\mathbf{C}_1 = \mathbf{B}(\theta)\mathbf{C}_{\text{s}}\mathbf{B}^H(\theta) = \sum_{k=1}^{K} c_{4,s_k}\mathbf{b}(\theta_k)\mathbf{b}^H(\theta_k), \quad (14)$$

where $\mathbf{C}_{\text{s}} = \text{diag}(c_{4,s_1}, c_{4,s_2}, \ldots, c_{4,s_K})$ represents the cumulative matrix of the signal; $\mathbf{B} = [\mathbf{b}(\theta_1), \mathbf{b}(\theta_2), \ldots, \mathbf{b}(\theta_k)]$ represents the steering matrix; and its $k$th column can be represented as

$$\mathbf{b}(\theta_k) = \left[e^{jl_{-M}\gamma_k}, \ldots, 1, \ldots, e^{jl_M\gamma_k}\right]^T. \quad (15)$$

Obviously, (14) only contains DOA parameters, with which we can estimate DOA of all sources with $\mathbf{C}_1$.

*Definition 1:* (DOFs [23]) The number of DOFs of a sparse array is the cardinality of its difference coarray. Given a sparse array $\mathbb{L}$, $\mathbb{H}$ denotes the maximum consecutive segment of its difference coarray. The cardinality of $\mathbb{H}$ is named as the number of uniform DOFs of $\mathbb{L}$.

### 2.3. Mutual Coupling Model

In the absence of mutual coupling between array sensors, the expression of the received signal vector is the formula (8). However, in engineering practice, the mutual coupling between

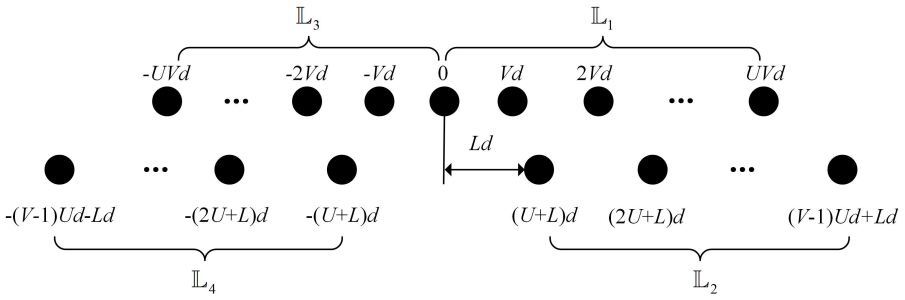


**FIGURE 2**. The symmetric shifted coprime array geometry.

array sensors must be fully considered. After discussing mutual coupling, the received signal model becomes

$$\mathbf{x}(t) = \mathbf{\Omega}\mathbf{A}_{\mathrm{FF}}\mathbf{s}_{\mathrm{FF}}(t) + \mathbf{\Omega}\mathbf{A}_{\mathrm{NF}}\mathbf{s}_{\mathrm{NF}}(t) + \mathbf{n}(t), \tag{16}$$

where $\mathbf{\Omega}$ represents the mutual coupling matrix of $Q \times Q$, describing the degree of coupling between two array sensors. Approximating the mutual coupling matrix $\mathbf{\Omega}$ to a B-band symmetric Toeplitz matrix [5],

$$\langle \mathbf{\Omega} \rangle_{m,n} = \begin{cases} c_{|l_m - l_n|}, & \text{if } |l_m - l_n| \le B \\ 0, & \text{otherwise} \end{cases} \tag{17}$$

where $c_0, c_1, c_2, \ldots, c_B$ represent the mutual coupling coefficient and satisfies $c_0 = 1 > |c_1| > |c_2|, \ldots, > |c_B|$. It is assumed that the greater the distance is between two sensors, the lower the mutual coupling is, then $|c_l/c_k| = l/k$. To evaluate the mutual coupling effect of arrays, the mutual coupling leakage coefficient $L_e$ can be expressed as

$$L_e = \frac{\|\mathbf{\Omega} - \mathrm{diag}(\mathbf{\Omega})\|_F}{\|\mathbf{\Omega}\|_F}. \tag{18}$$

The smaller the $L_e$ is, the stronger the overall anti-coupling ability of the array is. Usually, the bigger the spacing is between array elements, the smaller the mutual coupling leakage coefficient $L_e$ is. The focus of this article is on sparse array design and the use of data received by the antenna backend for array signal processing. Therefore, it is hoped that the larger the spacing between array elements, the better.

## 3. SYMMETRIC SHIFTED COPRIME ARRAY

In this section, we first give the structure of SSCA, then analyze the properties of SSCA and present the analytical expressions of degrees of freedom and weight functions.

### 3.1. Symmetric Shifted Coprime Array Structure

As shown in Fig. 2, the proposed SSCA consists of four subarrays, i.e., $\mathbb{L}_1$, $\mathbb{L}_2$, $\mathbb{L}_3$, and $\mathbb{L}_4$. $\mathbb{L}_1$ has $U+1$ sensors with inter-element spacing $V$, while $\mathbb{L}_2$ has $V-1$ sensors with inter-element spacing $U$, and it shifts to the right $L$ with respect to the $\mathbb{L}_1$. $\mathbb{L}_1$ and $\mathbb{L}_2$ are flipped around the origin to generate $\mathbb{L}_3$ and $\mathbb{L}_4$, respectively. The set of sensor positions $\mathbb{L}$ of SSCA can be expressed as

$$\begin{cases} \mathbb{L} = \mathbb{L}_1 \cup \mathbb{L}_2 \cup \mathbb{L}_3 \cup \mathbb{L}_4 \\ \mathbb{L}_1 = \{uV \mid u \in [0, U]\} \\ \mathbb{L}_2 = \{vU + L \mid v \in [1, V-1]\}, \\ \mathbb{L}_3 = -\mathbb{L}_1 \\ \mathbb{L}_4 = -\mathbb{L}_2 \end{cases} \tag{19}$$

where $L = \lfloor (U+1)/2 \rfloor V$.

### 3.2. Difference Co-Array of Symmetric Shifted Coprime Array

Firstly, we analyze the difference co-array of each subarray of SSCA and the relationship among them. Based on this, we make holes of the differences co-array filled as much as possible by selecting the appropriate value of $L$. Then, the maximum number of continuous virtual elements of SSCA is obtained.

According to (19), the differences co-array of SSCA is given by

$$\mathrm{diff}(\mathbb{L}, \mathbb{L}) = \cup \mathrm{diff}(\mathbb{L}_i, \mathbb{L}_j), \quad i, j \in \{1, 2, 3, 4\}, \tag{20}$$

where $\mathrm{diff}(L_i, L_j) = \{a - b \mid a \in L_i, b \in L_j\}$. Because of $\mathbb{L}_1 = -\mathbb{L}_3$ and $\mathbb{L}_2 = -\mathbb{L}_4$, we have

$$\begin{cases} \mathrm{diff}(\mathbb{L}_2, \mathbb{L}_1) = -\mathrm{diff}(\mathbb{L}_1, \mathbb{L}_2), \\ \mathrm{diff}(\mathbb{L}_2, \mathbb{L}_3) = -\mathrm{diff}(\mathbb{L}_4, \mathbb{L}_1), \\ \mathrm{diff}(\mathbb{L}_3, \mathbb{L}_1) = -\mathrm{diff}(\mathbb{L}_1, \mathbb{L}_3), \\ \mathrm{diff}(\mathbb{L}_3, \mathbb{L}_2) = -\mathrm{diff}(\mathbb{L}_1, \mathbb{L}_4), \\ \mathrm{diff}(\mathbb{L}_3, \mathbb{L}_3) = -\mathrm{diff}(\mathbb{L}_1, \mathbb{L}_1), \\ \mathrm{diff}(\mathbb{L}_3, \mathbb{L}_4) = -\mathrm{diff}(\mathbb{L}_1, \mathbb{L}_2), \\ \mathrm{diff}(\mathbb{L}_4, \mathbb{L}_1) = -\mathrm{diff}(\mathbb{L}_1, \mathbb{L}_4), \\ \mathrm{diff}(\mathbb{L}_4, \mathbb{L}_2) = -\mathrm{diff}(\mathbb{L}_2, \mathbb{L}_4), \\ \mathrm{diff}(\mathbb{L}_4, \mathbb{L}_3) = -\mathrm{diff}(\mathbb{L}_2, \mathbb{L}_1), \\ \mathrm{diff}(\mathbb{L}_4, \mathbb{L}_4) = -\mathrm{diff}(\mathbb{L}_2, \mathbb{L}_2). \end{cases} \tag{21}$$

Therefore, we focus on analyzing

$$\begin{cases} \mathrm{diff}(\mathbb{L}_1, \mathbb{L}_1) = \{uV \mid u \in [-U, U]\}, \\ \mathrm{diff}(\mathbb{L}_1, \mathbb{L}_2) = \{uV - vU - L \mid u \in [0, U],\ v \in [1, V-1]\}, \\ \mathrm{diff}(\mathbb{L}_1, \mathbb{L}_3) = \{uV \mid u \in [0, 2U]\}, \\ \mathrm{diff}(\mathbb{L}_1, \mathbb{L}_4) = \{uV + vU + L \mid u \in [0, U],\ v \in [1, V-1]\}, \\ \mathrm{diff}(\mathbb{L}_2, \mathbb{L}_2) = \{vU \mid v \in [2-V, V-2]\}, \\ \mathrm{diff}(\mathbb{L}_2, \mathbb{L}_4) = \{vU + 2L \mid v \in [2, 2V-2]\}. \end{cases} \tag{22}$$

To analyze the properties of $\mathrm{diff}(\mathbb{L}, \mathbb{L})$, we present *Propositions 1 to 4*.

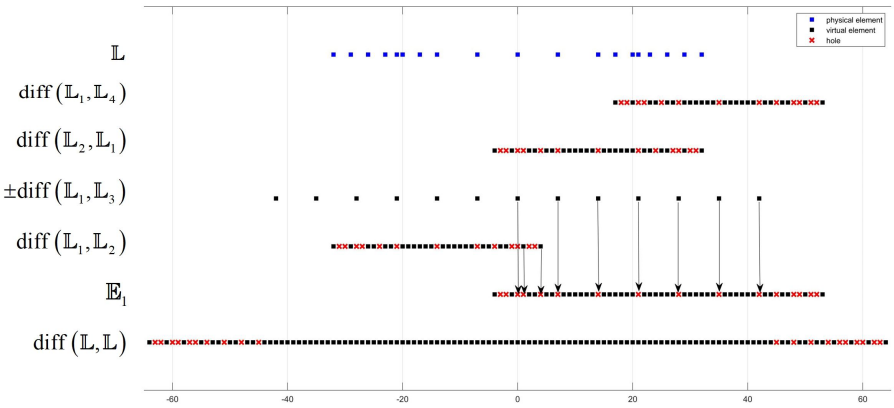


**FIGURE 3**. An example of SSCA configuration co-array, where $U = 3$, $V = 7$, $L = 14$.

*Proposition 1:* The relationship between sets diff $(\mathbb{L}_1, \mathbb{L}_4)$ and diff $(\mathbb{L}_2, \mathbb{L}_1)$ can be expressed as

$$\text{diff}\,(\mathbb{L}_1, \mathbb{L}_4) = \text{diff}\,(\mathbb{L}_2, \mathbb{L}_1) + UV. \tag{23}$$

*Proof*: See Appendix A.

*Proposition 2:* In the range of diff $(\mathbb{L}_2, \mathbb{L}_1)$, there are holes at the following location

$$\mathbb{P}_{2,1} = \mathbb{P}_1 \cup \lfloor (U+1)/2 \rfloor V \cup \mathbb{P}_2\ , \tag{24}$$

where

$$\begin{aligned} \mathbb{P}_1 \ &= \ \{aU + bV + L \mid a \geq 0,\ b > 0, \\ &\quad\ 0 < aU + bV < U(V-1)\}, \end{aligned} \tag{25}$$

$$\begin{aligned} \mathbb{P}_2 \ &= \ \{L - (cU + dV) \mid c \geq 0,\ d > 0, \\ &\quad\ 0 < cU + dV < U(V-1)\}. \end{aligned} \tag{26}$$

*Proof*: See Appendix B.

*Proposition 3:* In the diff$(\mathbb{L}_1, \mathbb{L}_4)$ range, there are holes located at

$$\mathbb{P}_{1,4} = \mathbb{P}_3 \cup \{UV + \lfloor (U+1)/2 \rfloor V\} \cup \mathbb{P}_4, \tag{27}$$

where $\mathbb{P}_3 = \mathbb{P}_1 + UV,\ \mathbb{P}_4 = \mathbb{P}_2 + UV$.

*Proof*: See Appendix C.

*Proposition 4:* Let $\mathbb{E}_1 = \text{diff}(\mathbb{L}_1, \mathbb{L}_4) \cup \text{diff}(\mathbb{L}_2, \mathbb{L}_1)$, and the positions where there are holes in set $\mathbb{E}_1$ are

$$\mathbb{P}_{e_1} = \mathbb{P}_2 \cup \mathbb{P}^r_{1,4} \cup \mathbb{P}_3 \cup \{L, UV + L\}, \tag{28}$$

where

$$\mathbb{P}^r_{1,4} = \{\alpha V + L \mid L < \alpha V + L < UV + L\}. \tag{29}$$

*Proof*: See Appendix D.

According to (22), we know that the position of the elements in $\pm\,\text{diff}(\mathbb{L}_1, \mathbb{L}_3)$ are independent of $L$. To increase the number of continuous virtual elements of the proposed array, we choose $L = \lfloor (U+1)/2 \rfloor V$ to make the holes in $\mathbb{E}_1$ filled by the elements in $\pm\,\text{diff}(\mathbb{L}_1, \mathbb{L}_3)$ as much as possible. Therefore, we have the following *Proposition*.

*Proposition 5:* The maximum number of continuous virtual elements provided by a shifted coprime array is given by

$$\mathbb{H}_e = [-UV - U - V - L, \quad UV + U + V + L]. \tag{30}$$

*Proof*: See Appendix E.

To illustrate *Propositions 1 to 5* more intuitively, Fig. 3 shows an example of SSCA, where blue squares denote the physical element of SSCA; black squares represent virtual elements; red squares stand for holes. The number of sensors $Q = 10$, array parameters $(U, V) = (3, 7)$, $L = 14$; therefore, the set of physical array positions is $\mathbb{L} = \{-32, -29, -26, -23, -21, -20, -17, -7, 0, 7, 14, 17, 20, 21, 23, 26, 29, 32\}$.

As can be seen from Fig. 3, the hole in the diff$(\mathbb{L}_2, \mathbb{L}_1)$ range is located in $\mathbb{P}_{2,1} = \{-3, -2, 0, 1, 4, 7, 14, 21, 24, 27, 28, 30, 31\}$, while the hole in the diff$(\mathbb{L}_1, \mathbb{L}_4)$ range is located at $\mathbb{P}_{1,4} = \{18, 19, 21, 22, 25, 28, 35, 42, 45, 48, 49, 51, 52\}$. Therefore, diff$(\mathbb{L}_1, \mathbb{L}_4)$ can be seen as each element of diff$(\mathbb{L}_2, \mathbb{L}_1)$ plus the $UV$ generated set, indicating that diff$(\mathbb{L}_2, \mathbb{L}_1)$ and diff$(\mathbb{L}_1, \mathbb{L}_4)$ have a similar virtual array structure. The holes in the $\mathbb{E}_1$ range are located at $\mathbb{P}_{e_1} = \{-3, -2, 0, 1, 4, 7, 14, 21, 28, 35, 42, 45, 48, 49, 51, 52\}$, in which $\{0, 7, 14, 21, 28, 35, 42\}$ are filled by diff$(\mathbb{L}_1, \mathbb{L}_3)$. The holes at $\{1, 4\}$ are filled by diff$(\mathbb{L}_1, \mathbb{L}_2)$. Therefore, the first hole in the virtual array is located at $\{45\}$, and the number of continuous virtual array elements generated by the SSCA array is 89.

### 3.3. Weight Functions

The effect of mutual coupling is considerably related to the element spacing. According to [6], weight functions $w(1)$, $w(2)$, $w(3)$ can be used to evaluate the effect of mutual coupling. The first three weight functions of the SSCA are given by *Proposition 6*.

*Proposition 6:* The weight function of the SSCA can be expressed as

$$w(1) = w(2) = w(3) = 2. \tag{31}$$

*Proof:* Let's first prove that there are $(U+1)(V-1)$ different elements of diff$(\mathbb{L}_1, \mathbb{L}_2)$. According to Equation (22) diff$(\mathbb{L}_1, \mathbb{L}_2) = \{uV - vV - L \mid u \in [0, U], v \in [1, V-1]\}$ and diff$(\mathbb{L}_1, \mathbb{L}_2) = -\,\text{diff}(\mathbb{L}_2, \mathbb{L}_1)$. Let's say that there are two identical elements in diff$(\mathbb{L}_1, \mathbb{L}_2)$, then the following formula holds

$$u_1V - v_1U - L = u_2V - v_2U - L \Rightarrow \frac{v_1 - v_2}{u_1 - u_2} = \frac{V}{U}, \tag{32}$$

where $0 \le u_1, u_2 \le U$, $1 \le v_1, v_2 \le V-1$. Since $v_1 - v_2 < V$, $U$ and $V$ are coprime, Equation (32) cannot be established. Therefore, there are no repeating elements in $\text{diff}(\mathbb{L}_1, \mathbb{L}_2)$, that is, there are $(U+1)(V-1)$ different elements.

Then, it is proved that when $L = (U+1)V/2$, there are no identical elements between sets $\text{diff}(\mathbb{L}_1, \mathbb{L}_2)$ and $\text{diff}(\mathbb{L}_2, \mathbb{L}_1)$. Assuming that the same elements exist in both sets, the following equation holds

$$u_1 V - v_1 U - L = v_2 U + L - u_2 V, \tag{33}$$

where $0 \le u_1, u_2 \le U$, $1 \le n_1, n_2 \le V-1$. Substituting $L = (U+1)V/2$ into (33) yields

$$\frac{u_1 + u_2 - U - 1}{v_1 + v_2} = \frac{U}{V}. \tag{34}$$

Since $u_1 + u_2 - U - 1 < U$, $U$ and $V$ are coprime, there is no integer to make (34) true.

### 3.4. Compared with Other Arrays

SSCA performance is quantified by comparing it with SNAI [28], SDNA [31], and SNAII [30] in two aspects, the number of consecutive lags and mutual coupling leakage coefficient.

As shown in Table 1, when numbers of sensors are equal, the number of consecutive lags of SSCA is obviously larger than that of SNAI and SDNA, and it is smaller than SNAII. But SSCA has stronger anti-coupling ability than SNAII, which can be seen in Table 2.

**TABLE 1**. The number of consecutive lags for different arrays.

| Sensors number | SNAI | SDNA | SNAII | SSCA |
|---|---|---|---|---|
| 31 | 112 | 141 | 239 | 229 |
| 35 | 163 | 177 | 305 | 277 |
| 37 | 181 | 196 | 379 | 317 |
| 39 | 201 | 217 | 379 | 341 |

**TABLE 2**. Mutual coupling leakage coefficient with $c_1 = 0.3$.

| Sensors number | SNAI | SDNA | SNAII | SSCA |
|---|---|---|---|---|
| 31 | 0.3607 | 0.3394 | 0.3577 | 0.2791 |
| 35 | 0.3597 | 0.3408 | 0.3573 | 0.2647 |
| 37 | 0.3508 | 0.3503 | 0.3492 | 0.2539 |
| 39 | 0.3589 | 0.3420 | 0.3569 | 0.2508 |

It can be seen from Table 2 that under the same number of physical array elements, SSCA can obtain the lower mutual coupling leakage coefficient than SNAI, SDNA, and SNAII, because the SSCA structure is more sparse. This means that the SSCA can obtain higher accuracy for DOA and distance estimation.

## 4. THE PROPOSED ALGORITHM

This section mainly introduces the parameter solving method of mixed field sparse matrix. The solution method is spatial smoothing MUSIC (SS-MUSIC) algorithm [34]. Based on MUSIC algorithm and spatial smoothing technology, this algorithm smooths the received data of continuous virtual array generated by difference coarray and then uses MUSIC algorithm to estimate the parameters.

### 4.1. DOA Estimation

The cumulant matrix $\mathbf{C}_1$ is vectorized, and the continuous virtual elements in $\mathbf{C}_1$ are extracted for column vectorization

$$\begin{aligned} \bar{\mathbf{z}} &= \text{vec}\left\{\mathbf{C}_1\right\} = \text{vec}\left[\sum_{k=1}^{K} c_{4,s_k}\left(\mathbf{b}\left(\theta_k\right)\mathbf{b}^H\left(\theta_k\right)\right)\right] \\ &= \left(\mathbf{B}^* \odot \mathbf{B}\right)\mathbf{p} = \overline{\mathbf{B}}_1 \mathbf{p}, \end{aligned} \tag{35}$$

where $\overline{\mathbf{B}}_1 = [\overline{\mathbf{b}}_1(\theta_1), \overline{\mathbf{b}}_1(\theta_2), \ldots, \overline{\mathbf{b}}_1(\theta_k)]$ is the virtual array's equivalent manifold matrix. Vector $\bar{\mathbf{z}}$ is a single snapshot data, and when multiple signals are incident on the array, decorrelation operation is required. The commonly used decorrelation method is spatial smoothing.

Assume that the dimension of vector $\bar{\mathbf{z}}$ is $2L_z+1$, that is, the continuous virtual array range is $[-L_z, L_z]$. Divide the vector $\bar{\mathbf{z}}$ into $L_z+1$ overlapping subvectors, with each containing $L_z+1$ elements. The $i$th subvector $\bar{\mathbf{z}}_i$ is the $i$th element to the $i+L_z$ element of the vector $\bar{\mathbf{z}}$. Calculate the covariance matrix of each subvector and average it to obtain

$$\overline{\mathbf{R}}_{ss} = \frac{1}{L_z+1}\sum_{i=1}^{L_z+1}\overline{\mathbf{R}}_i = \frac{1}{L_z+1}\sum_{i=1}^{L_z+1}\left(\bar{\mathbf{z}}_i\bar{\mathbf{z}}_i^H\right). \tag{36}$$

After the above spatial smoothing operation, the DOA information of the mixed field can be solved using the classical subspace algorithm based on the covariance matrix $\overline{\mathbf{R}}_{ss}$

$$\overline{\mathbf{R}}_{ss} = \mathbf{E}_S\mathbf{\Lambda}_S\mathbf{E}_S^H + \mathbf{E}_N\mathbf{\Lambda}_N\mathbf{E}_N^H. \tag{37}$$

In (37), $\mathbf{E}_S$ and $\mathbf{E}_N$ represent the eigenvectors corresponding to the large and small eigenvalues, respectively. According to the basic idea of MUSIC method, the following spectral peak search formula can be obtained

$$G(\theta) = \frac{1}{\overline{\mathbf{b}}_1^H\left(\theta_k\right)\mathbf{E_N}\mathbf{E_N}^H\overline{\mathbf{b}}_1\left(\theta_k\right)}. \tag{38}$$

### 4.2. Estimating Distance

The estimated DOA angle value of the mixing field is $\{\hat{\theta}_k, k = 1, \ldots, K\}$, and by sequentially inputting the estimated angle values into spectral peak search function, the distance parameters of the corresponding near-field in the mixed field can be obtained

$$\bar{r}_k = \min_r\left[\mathbf{a}^H\left(\hat{\theta}_k, r\right)\overline{\mathbf{U}}_n\overline{\mathbf{U}}_n^H\mathbf{a}\left(\hat{\theta}_k, r\right)\right]^{-1}, \tag{39}$$

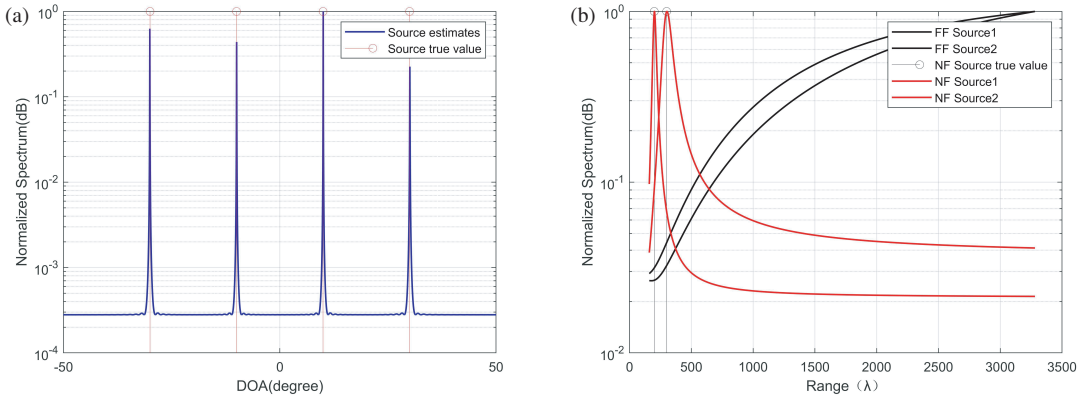


**FIGURE 4**. Normalized spatial spectrum of SSCA array. (a) Spatial spectrum for DOA estimation by using SSCA array. (b) Spatial spectrum for range estimation by using SSCA array.

where $\overline{\mathbf{U}}_n \in \mathbf{C}^{(2M+1)\times(2M+1-K)}$ is composed of eigenvectors of $\mathbf{R} = \mathrm{E}\{\mathbf{x_i}(t)\mathbf{x_i}^H(t)\}$ corresponding to the $(2M+1-K)$ smallest eigenvalues. According to the set distance range, it is easy to identify the near-field and far-field sources in the mixed field. When $\bar{r}_k \in [0.62(\mathrm{D}^3/\lambda)^{1/2}, 2\mathrm{D}^2/\lambda]$, the $k$th source is a near-field one. When $\bar{r}_k > 2D^2/\lambda$, the $k$th source is far field. Therefore, we easily distinguish NF and FF targets.

After summarizing the principle of the algorithms mentioned above, the localization of mixed NF and FF sources algorithm based on fourth-order cumulants proposed in this paper is calculated in Table 3 which describes the method.

**TABLE 3**. Implementation steps of mixed NF and FF sources localization algorithm based on fourth-order cumulants.

| |
|---|
| **Input:** the signals received by physical sensors $\mathbf{x}(t)$. |
| **Output:** DOA and distance estimation $(\hat{\theta}_k, \bar{r}_k)$. |
| Specific algorithm steps: |
| 1: Calculate the fourth-order cumulants matrix $\mathbf{C}_1$ via (14). |
| 2: Vectoring $\mathbf{C}_1$ to generate $\bar{\mathbf{z}}$ via (35). |
| 3: According to (36), calculate a spatial smoothing matrix $\overline{\mathbf{R}}_{ss}$. |
| 4: Calculate $\mathbf{E}_N$ via (37). |
| 5: Obtaining DOA estimates $\hat{\theta}_k$ via (38). |
| 6: Calculate $\overline{\mathbf{U}}_n$, and obtaining distance estimates $\bar{r}_k$ via (39). |

## 5. RESULTS OF THE SIMULATION

In order to verify the performance of the proposed SSCA for localization of mixed field sources simulations are conducted. Firstly, we present the weight functions of the proposed SSCA, SNAI [28], SDNA [29], and SNAII [30]. Secondly, we simulate the root mean square error (RMSE) of different signal-to-noise ratios (SNRs), the number of snapshots, and level of mutual coupling. The RMSE is defined as

$$\mathrm{RMSE} = \sqrt{\frac{1}{\tilde{K}N}\sum_{i=1}^{N}\sum_{k=1}^{\tilde{K}}\left(\hat{a}_k^i - a_k\right)^2}, \tag{40}$$

where $N = 2000$ is the number of Monte Carlo trials; $a_k$ represents the true DOA or range of the $k$th source; $\hat{a}_k^i$ is the estimated DOA or distance of the $i$th source obtained from the $k$-th trial. For the RMSE of near-field sources, we can set $\tilde{K} = K_1$, while for that of far-field sources, $\tilde{K} = K - K_1$.

1) **Music Spectral:** In this simulation, we assume that four sources are incident on the SSCA with $Q = 29$. The directions and ranges of the four mixed field sources are $(-30°, 200\lambda)$, $(-10°, 300\lambda)$, $(10°, \infty)$, and $(30°, \infty)$. Fixed parameters are set to SNR = 10 dB, $T = 1000$ snapshot. Fig. 4 shows the spatial spectra of signal DOA parameter estimation and distance parameter estimation in turn. In Fig. 4(a), the DOA values of the above four mixed sources are estimated. Fig. 4(b) presents the spectral obtained by searching the spectral peak of the signal distance in the Fresnel region by substituting different DOA estimates. The two red lines in the figure have peaks within the search range, which are the distance estimates of the two near-field sources. The two black lines have no peaks within the search range of near-field sources, indicating that the corresponding signal source is located in the far-field source.

2) **Weight Functions:** In this simulation, we set the number of sensors $Q = 29$. Fig. 5 shows the weight functions of SNAI, SDNA, SNAII, and the proposed SSCA. It can be seen that, for the SNAI, SDNA, and SNAII, their weight functions are $w(1) = 16, w(2) = 15, w(3) = 14$, $w(1) = 14, w(2) = 13, w(3) = 12$, and $w(1) = 14, w(2) = 13, w(3) = 12$, respectively. This can be attributed to their design originating from nested arrays, which have a relatively dense array structure. Compared with other three arrays, the weight functions of SSCA are much smaller, which are $w(1) = 2$, $w(2) = 2$, $w(3) = 2$, leading to stronger anti-mutual coupling ability of SSCA.

3) **RMSE Performance:** The following simulations focus on the relationship between RMSE performance and the input SNR, number of snapshots, and $c_1$ modulus of the coupling coefficient. The mutual coupling model is characterized by $B = 100$, $c_1 = 0.3e^{j\pi/3}$, $c_l = c_1 e^{-j(l-1)\pi/8}/l$ (except in the case of changes in $c_1$). Fixed parameters are set to SNR = 10 dB, $T = 500$ snapshots. The directions and ranges of the four mixed field sources are $(-30°, 200\lambda)$, $(-10°, 300\lambda)$, $(10°, \infty)$ and $(30°, \infty)$.

Figure 6 presents the RMSEs versus SNR for the four kinds of sparse arrays. As can be seen from Fig. 6, when SNR is less

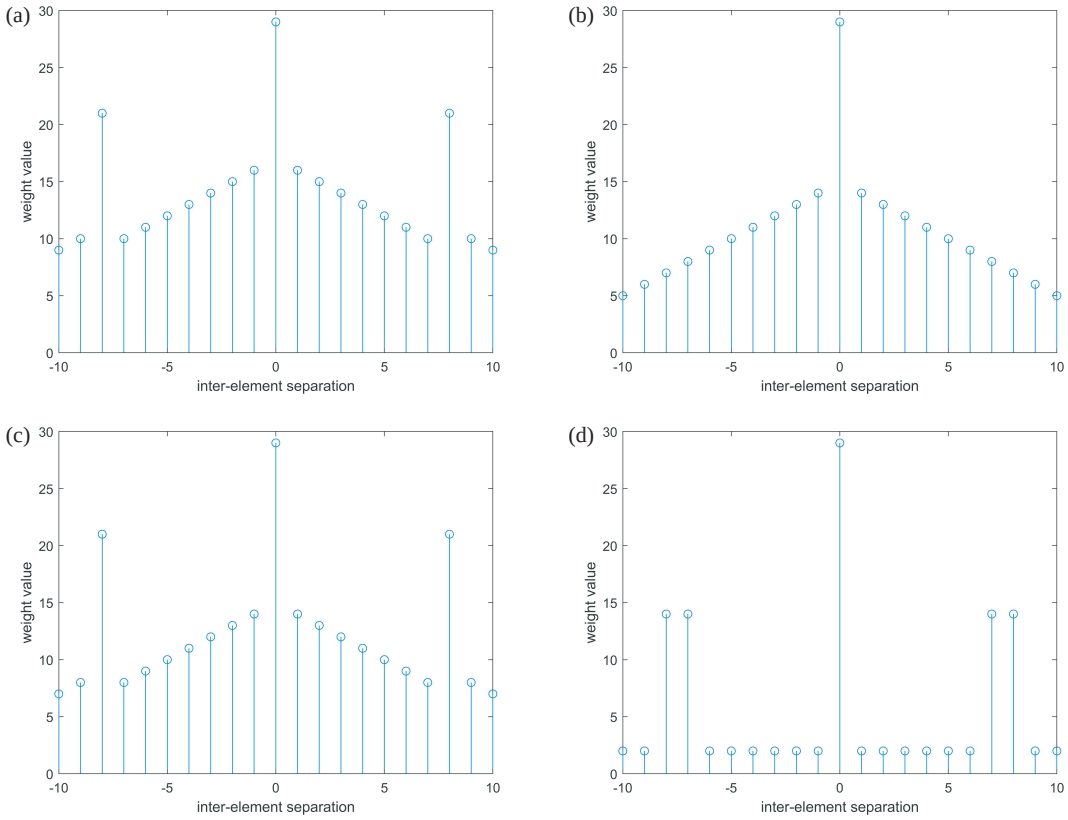


**FIGURE 5**. The weight functions for four kinds of SLAs. (a) SNAI. (b) SNAII. (c) SDNA. (d) SSCA.

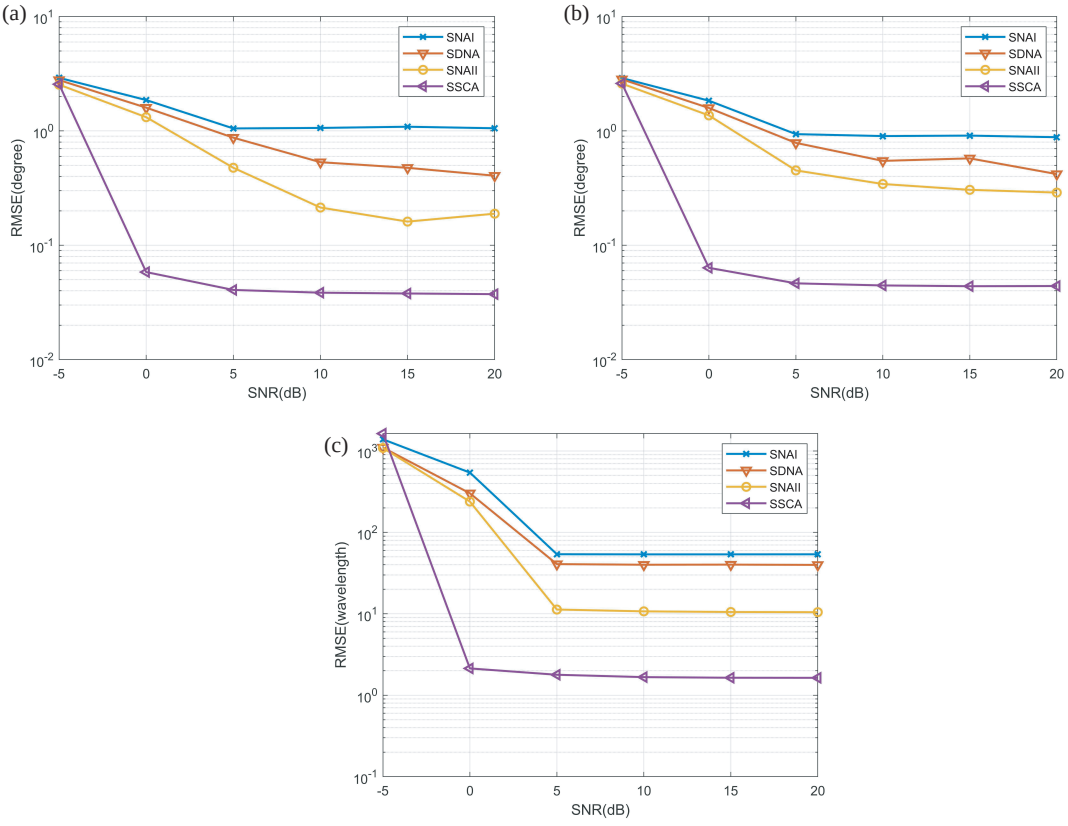


**FIGURE 6**. RMSE curves for DOA estimation and distance estimation under different SNR. (a) DOA estimations for FF sources. (b) DOA estimations for NF sources. (c) Range estimations.

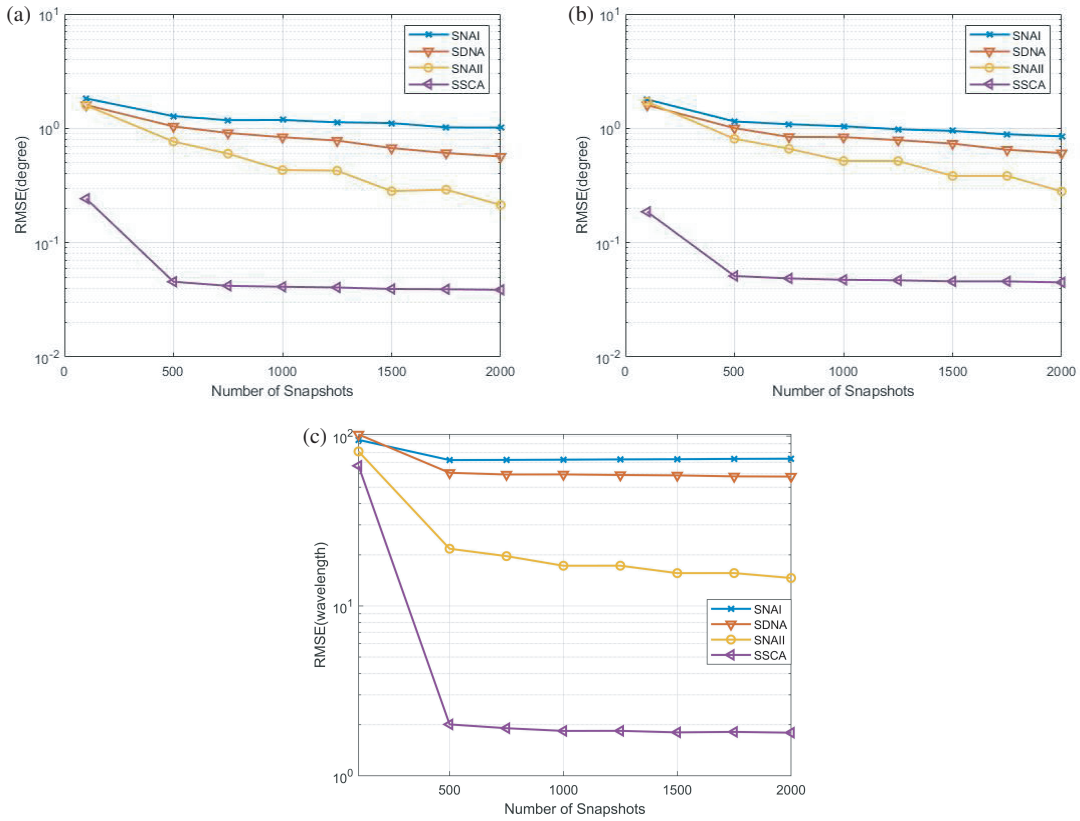


**FIGURE 7**. RMSE curves for DOA estimation and distance estimation under different Snapshots. (a) DOA estimations for FF sources. (b) DOA estimations for NF sources. (c) Range estimations.

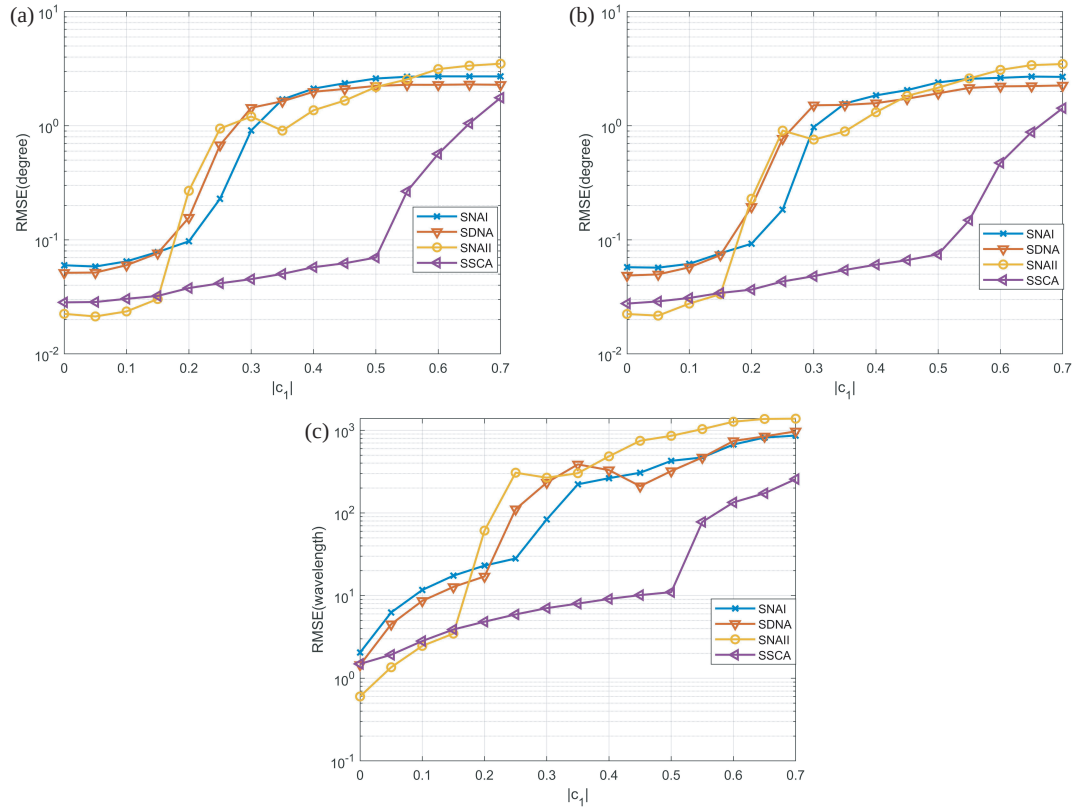


**FIGURE 8**. RMSE curves for DOA estimation and distance estimation under different $|c_1|$. (a) DOA estimations for FF sources. (b) DOA estimations for NF sources. (c) Range estimations.

than 5 dB, the RMSE curves of SSCA array present a downward trend, while the decline trend of SNAI, SDNA and SNAII is not obvious. When the SNR exceeds 5 dB, the RMSE curves are relatively stable. This is because mutual coupling has become an important factor hindering estimation performance improvement. In addition, we see that the RMSE curve of the proposed SSCA is the lowest among the four arrays, indicating that the proposed array can provide the most excellent estimation performance among them. This is attributed to the proposed array having good anti mutual coupling ability.

Figure 7 shows the RMSE curves of DOA and ranges for mixed field sources under different snapshots. From Fig. 7, it can be seen that RMSE curves of all arrays show a downward trend with the increase of the number of snapshots, and SSCA arrays show an obvious downward trend, with more accurate estimation accuracy. The RMSE curves of other arrays change slowly with the increase of number of snapshots due to the influence of mutual coupling. When number of snapshots $T \geq 500$, the RMSE curve of SSCA array becomes stable, which indicates that the increase of number of snapshots has no decisive effect on the estimation accuracy of DOA parameters.

The RMSE of DOA and range estimates versus mutual coupling coefficient $|c_1|$ is shown in Fig. 8. With the increase of $|c_1|$, the RMSE curves of all arrays show an increasing trend, and the parameter estimation performance deteriorates gradually. This is because the larger the mutual coupling coefficient $|c_1|$ is, the more serious the mutual coupling leakage is between the array elements. Additionally, we see that when the mutual coupling coefficient $|c_1| = 0$, SNAII array has the highest estimation accuracy. The reason for this is that if $|c_1| = 0$, the performance curves of DOA parameter estimation are determined by the number of consecutive lags generated by the array, while SNAII array can provide more consecutive lags than other three arrays. When the mutual coupling coefficient $|c_1| > 0.2$, the RMSE curves of SNAI, SDNA, and SNAII rise significantly, while the RMSE curves of SSCA arrays do not change significantly. When $|c_1| > 0.5$, the RMSE curves of SSCA show an upward trend, but the parameter estimation performance of SSCA arrays is still better than that of the other three sparse arrays. It indicates that the proposed SSCA outperforms other arrays when the mutual coupling is very severe.

## 6. CONCLUSION

In this article, we propose a symmetric shifted coprime array for localization of far-field and near-field sources. For the proposed array, the analytical expression is provided, which makes the array design convenient. The DOFs of the proposed array are improved, and the sensor pairs with small inter-element spacing are reduced by translating the subarray of the traditional prime array. The expressions of DOFs and weight functions of the proposed array are also derived. The first three weight functions of SSCA are $w(1) = w(2) = w(3) = 2$, which are less than the weight functions of SNAI, SDNA, and SNAII. Numerical results show that the anti-coupling ability of proposed array is improved while the DOFs are guaranteed. Therefore, it has higher DOA and range estimation accuracy than existing arrays. However, because the statistics used are fourth-order cumulants, it will bring relatively high computational complexity.

## APPENDIX A. PROOF OF PROPOSITION 1

Any element in set $\text{diff}(\mathbb{L}_2, \mathbb{L}_1)$ is $d_{2,1}$. According to formula (22), $d_{2,1}$ can be represented as

$$d_{2,1} = v_1 U - u_1 V + L \tag{A1}$$

where $1 \leq v_1 \leq V-1, 0 \leq u_1 \leq U$. Adding $UV$ to $d_{2,1}$ gives

$$d_{2,1} + UV = v_2 U + u_2 V + L = \text{diff}(\mathbb{L}_1, \mathbb{L}_4), \tag{A2}$$

where $v_1 = v_2$ and $u_2 = U - u_1$. According to (22), it can be concluded that $\{d_{2,1} + UV\} \in \text{diff}(\mathbb{L}_1, \mathbb{L}_4)$. Similarly, it can be proven that $\{d_{1,4} - UV\} \in \text{diff}(\mathbb{L}_2, \mathbb{L}_1)$, where $d_{1,4}$ represents any element in set $\text{diff}(\mathbb{L}_1, \mathbb{L}_4)$.

## APPENDIX B. PROOF OF PROPOSITION 2

Here, contradiction is used to show that element $p_1$ in $\mathbb{P}_1$ does not belong to set $\text{diff}(\mathbb{L}_2, \mathbb{L}_1)$. Supposing $p_1 \in \text{diff}(\mathbb{L}_2, \mathbb{L}_1)$, then the following equation is obtained

$$aU + bV + L = vU + L - uV, \tag{B1}$$

where $a \geq 0$, $b \geq 0$, $1 \leq v \leq V-1$, and $0 \leq u \leq U$. The following conclusion can be derived from (B1)

$$\frac{U}{V} = \frac{u+b}{v-a}. \tag{B2}$$

Because of $v - a < V$ and the coprime of $U$ and $V$, there is no integer $u$ that satisfies Equation (B2). Therefore, assume that $p_1 \in \text{diff}(\mathbb{L}_2, \mathbb{L}_1)$ does not hold, that is, the elements located in set $\mathbb{P}_1$ are holes within the range of $\text{diff}(\mathbb{L}_2, \mathbb{L}_1)$. Similarly, it can be proven that the sets $\{L\}$ and $\mathbb{P}_2$ are also holes within the range of $\text{diff}(\mathbb{L}_2, \mathbb{L}_1)$.

## APPENDIX C. PROOF OF PROPOSITION 3

By proving $p_1 \notin \text{diff}(\mathbb{L}_2, \mathbb{L}_1)$ in *Propositions 2*, $\{h_1 + UV\} \notin \text{diff}(\mathbb{L}_2, \mathbb{L}_1) + UV$ is obtained. According to *Propositions 1*, $\text{diff}(\mathbb{L}_1, \mathbb{L}_4) = \text{diff}(\mathbb{L}_2, \mathbb{L}_1) + UV$, $\{h_1 + UV\} \notin \text{diff}(\mathbb{L}_1, \mathbb{L}_4)$ can be obtained. Therefore, the virtual array corresponding to the set $\text{diff}(\mathbb{L}_1, \mathbb{L}_4)$ can be generated by the virtual array corresponding to $\text{diff}(\mathbb{L}_2, \mathbb{L}_1)$ moving to the right $UV$, and holes in set $\text{diff}(\mathbb{L}_1, \mathbb{L}_4)$ can be obtained by shifting $\mathbb{P}_1$, $\mathbb{P}_2$, and $\{L\}$ to the right $UV$.

## APPENDIX D. PROOF OF PROPOSITION 4

The range of values of elements in sets $\text{diff}(\mathbb{L}_1, \mathbb{L}_4)$ and $\text{dif}(\mathbb{L}_2, \mathbb{L}_1)$ can be obtained according to Equations (21) and (22)

$$\begin{cases} U + L \leq d_{1,4} \leq UV + U(V-1) + L, \\ L - U(V-1) \leq d_{2,1} \leq U(V-1) + L, \end{cases} \tag{D1}$$

where $d_{1,4} \in \text{diff}(\mathbb{L}_1, \mathbb{L}_4)$, $d_{2,1} \in \text{diff}(\mathbb{L}_2, \mathbb{L}_1)$. Therefore, there is a range of overlap between $\text{diff}(\mathbb{L}_1, \mathbb{L}_4)$ and $\text{diff}(\mathbb{L}_2, \mathbb{L}_1)$, which can be given by

$$\mathbb{H}_1 = \{h_1 \mid U + L \leq h_1 \leq U(V-1) + L\}. \tag{D2}$$

Within this overlap, some holes in $\mathbb{P}_{2,1}$ may be filled by elements in diff$(\mathbb{L}_1, \mathbb{L}_4)$, while some holes in $\mathbb{P}_{1,4}$ may also be filled by elements in diff$(\mathbb{L}_2, \mathbb{L}_1)$. Therefore, the next step is to explore which holes are filled and which remain in the diff$(\mathbb{L}_1, \mathbb{L}_4) \cup$ diff$(\mathbb{L}_2, \mathbb{L}_1)$ range. The values of elements in the sets $\mathbb{P}_1$, $\mathbb{P}_2$, $\mathbb{P}_3$, and $\mathbb{P}_4$ can be obtained from *Propositions 2 and 3*

$$\begin{cases} L < p_1 < L + U(V-1) \\ L - U(V-1) < p_2 < L \\ L + UV < p_3 < L + 2UV - U \\ L + U < p_4 < L + UV, \end{cases} \tag{D3}$$

where $p_1 \in \mathbb{P}_1$, $p_2 \in \mathbb{P}_2$, $p_3 \in \mathbb{P}_3$, and $p_4 \in \mathbb{P}_4$. The overlap range in Equation (D2) is compared with the range of hole (D3)

$$\begin{cases} \mathbb{H}_1 \cap \mathbb{P}_1 \neq \varnothing \\ \mathbb{H}_1 \cap \mathbb{P}_2 = \varnothing \\ \mathbb{H}_1 \cap \mathbb{P}_3 = \varnothing \\ \mathbb{H}_1 \cap \mathbb{P}_4 \neq \varnothing \\ \mathbb{H}_1 \cap \{L, UV + L\} = \varnothing. \end{cases} \tag{D4}$$

which indicates that some holes in $\mathbb{P}_1$ may be filled by diff$(\mathbb{L}_1, \mathbb{L}_4)$, while some holes in $\mathbb{P}_4$ may be filled by diff$(\mathbb{L}_2, \mathbb{L}_1)$. Assuming that some holes in $\mathbb{P}_1$ can be filled by diff$(\mathbb{L}_1, \mathbb{L}_4)$, the following equation is true.

$$aU + bV + L = vU + uV + L. \tag{D5}$$

Next, the discussion (D5) is divided into two cases: $a > 0$ and $a = 0$. When $a > 0$, $U + V + L < h_1 < U(V-1) + L$ is obtained according to Equation (25), indicating that $p_1$ is in the overlapping range $\mathbb{H}_1$. If $a \neq n$, then Equation (D5) can be rewritten as

$$\frac{u-b}{a-v} = \frac{U}{V}. \tag{D6}$$

Because of $u - b < U$ and the coprime of $U$ and $V$, Equation (D6) cannot be established. Similarly, Equation (D5) is not valid for $b \neq u$. Therefore, Equation (D5) holds if $a = v$ and $b = u$. It can be further inferred that when $a > 0$, the hole located in $\mathbb{P}_1$ can be filled with elements from diff $(\mathbb{L}_1, \mathbb{L}_4)$. When $a = 0$, Equation (D5) can be rewritten as

$$bV = vU + uV \Rightarrow \frac{b-u}{v} = \frac{U}{V}. \tag{D7}$$

Because of $v - a < V$ and the coprime of $U$ and $V$, Equation (D7) cannot be established. It means that when $a = 0$, holes located in $\mathbb{P}_1$ cannot be filled by elements in diff$(\mathbb{L}_1, \mathbb{L}_4)$. Thus, after being filled with elements from diff$(\mathbb{L}_1, \mathbb{L}_4)$, the remaining elements in the set $\mathbb{P}_1$ can be represented as

$$\mathbb{P}_1^r = \{aV + L \mid L < \alpha V + L < U(V-1)\}. \tag{D8}$$

Similarly, after being filled by diff$(\mathbb{L}_2, \mathbb{L}_1)$, the remaining holes in $\mathbb{P}_4$ are located at

$$\mathbb{P}_4^r = \{aV + L \mid L + U < \alpha V + L < UV + L\}. \tag{D9}$$

The combination of (D8) and (D9) is obtained

$$\mathbb{P}_1^r \cup \mathbb{P}_4^r = \{aV + L \mid L < \alpha V + L < UV + L\}. \tag{D10}$$

Moreover, because the intersection of overlapping regions $\mathbb{H}_1$ and $\mathbb{P}_2 \cup \mathbb{P}_3 \cup \{L, UV + L\}$ is empty, the holes in the $\mathbb{P}_2 \cup \mathbb{P}_3 \cup \{L, UV + L\}$ region do not change at all.

## APPENDIX E. PROOF OF PROPOSITION 5

Let $L = gV$. Depending on whether $c$ is zero, the set $\mathbb{P}_2$ can be divided into

$$\mathbb{P}_2 = \mathbb{P}_2^1 \cup \mathbb{P}_2^2, \tag{E1}$$

where

$$\begin{aligned} \mathbb{P}_2^1 &= \{L - (cU + dV) \mid c > 0,\ d > 0, \\ &\quad 0 < cU + dV < U(V-1)\}, \end{aligned} \tag{E2}$$

$$\mathbb{P}_2^2 = \{\bar{d}V \mid -U(V-1) + L < \bar{d}V < L\}, \tag{E3}$$

where $\bar{d} = g - d$, $d > 0$. Then the union of the sets $\mathbb{P}_{1,4}^r$, $\mathbb{P}_2^2$, and $\{L, UV + L\}$ can be expressed as

$$\mathbb{P}_g = \{\alpha V \mid -U(VN - 1) + L < \alpha V < UV + L\}. \tag{E4}$$

Therefore, the hole in the $\mathbb{E}_1$ range can be rewritten as

$$\mathbb{P}_{ds} = \mathbb{P}_2^1 \cup \mathbb{P}_3 \cup \mathbb{P}_g. \tag{E5}$$

Next, the proof discusses sets $\mathbb{P}_g$, $\mathbb{P}_2^1$, and $\mathbb{P}_3$ in turn.

First, according to Equation (22) and $\pm$diff$(\mathbb{L}_1, \mathbb{L}_3)) = \{uV \mid u \in [-2U, 2U]\}$, when $g$ is satisfied

$$0 < g \leq U, \tag{E6}$$

all holes in $\mathbb{P}_g$ can be filled by elements in set $\pm$ diff $(\mathbb{L}_1, \mathbb{L}_3)$. Secondly, the relationship between $\mathbb{P}_2^1$ and diff $(\mathbb{L}_1, \mathbb{L}_2)$ will be analyzed below. According to Equation (22), the overlap range of the mirror images of sets diff $(\mathbb{L}_1, \mathbb{L}_2)$ and diff $(\mathbb{L}_2, \mathbb{L}_1)$ can be expressed as

$$\mathbb{H}_2 = \{h_2 \mid L - U(V-1) \leq h_2 \leq U(V-1) - L\}. \tag{E7}$$

Because $L < U(V-1)$, $\mathbb{H}_2 \neq \varnothing$, which indicates that holes in the diff $(\mathbb{L}_2, \mathbb{L}_1)$ range may be filled by elements in diff $(\mathbb{L}_1, \mathbb{L}_2)$.

Contrasting formulas (E2) and (E7) give an $\mathbb{H}_2 \cap \mathbb{P}_2^1 \neq \varnothing$. Suppose that there are holes in $\mathbb{P}_2^1$ that can be filled by the elements of set diff $(\mathbb{L}_1, \mathbb{L}_2)$, then the equation

$$-cU - dV + L = -vU - L + uV. \tag{E8}$$

Because of $c > 0$ and $d > 0$, $-U(V-1) + L < p_2^1 \leq L - U - V$ is obtained according to Equation (E2), where $p_2^1 \in \mathbb{P}_2^1$. If $p_2^1$ is in the overlapping region $\mathbb{H}_2$ and $c \neq v$, we get by substituting $L = gV$ into Equation (E8)

$$\frac{d + u - 2g}{v - c} = \frac{U}{V}. \tag{E9}$$

Because of $v - c < V$ and the coprime of $U$ and $V$, Equation (E8) cannot be established. Similarly, if $d + u \neq 2g$, Equation (E8) is not valid. Therefore, the conditions for formula (E8) are $c = v$ and $d + u = 2g$. It follows that the holes in $\mathbb{P}_2^1$ can all be filled by elements in diff $(\mathbb{L}_1, \mathbb{L}_2)$. However, as $L$ increases, some of $\mathbb{P}_2^1$'s holes will go beyond the overlap range $\mathbb{H}_2$ and cannot be filled by diff $(\mathbb{L}_1, \mathbb{L}_2)$. In order for all holes in A to be filled, conditions should be ensured

$$L - U - V \leq U(V-1) - L. \tag{E10}$$

Since $L = gV$ and $g$ are positive integers, according to Equation (E10), we obtain

$$0 < g \leq \left\lfloor \frac{U+1}{2} \right\rfloor. \tag{E11}$$

Finally, for $\mathbb{P}_3$, when $a = 0$ and $b = 1$, the minimum value $\mathbb{P}_3$ of $p_3^1$ can be expressed as $UV + gV + V$. In order for hole $h_3^1$ to be filled with elements from diff $(\mathbb{L}_1, \mathbb{L}_3)$, it is necessary to ensure $UV + gV + V \leq 2UV$, so we obtain

$$0 < g \leq U - 1. \tag{E12}$$

When $a = 1$ and $b = 1$, the second hole in $\mathbb{P}_3$ can be expressed as

$$p_3^2 = UV + U + V + gV. \tag{E13}$$

Next it will be shown that hole $p_3^2$ cannot be filled by elements of diff $(\mathbb{L}_1, \mathbb{L}_4)$. Assuming that $p_3^2$ can be filled with elements from diff $(\mathbb{L}_1, \mathbb{L}_4)$, there is a positive integer $n$ such that

$$U + V + UV + gV = 2uV \Rightarrow 2u - U - 1 = \frac{U}{V}. \tag{E14}$$

When $a = 1$ and $b = 1$, the second hole in $\mathbb{P}_3$ can be represented as

$$p_3^2 = UV + U + V + gV. \tag{E15}$$

Next it will be shown that hole $p_3^2$ cannot be filled by elements of diff $(\mathbb{L}_1, \mathbb{L}_3)$. Assuming that $p_3^2$ can be filled with elements from diff $(\mathbb{L}_1, \mathbb{L}_3)$, there is a positive integer $v$ such that

$$U + V + UV + gV = 2uV \Rightarrow 2u - U - 1 = \frac{U}{V}. \tag{E16}$$

Due to the coprime of $U$ and $V$, it is impossible to find an integer $u$ that holds Equation (E16). So $p_3^2$ cannot be filled with elements from diff $(\mathbb{L}_1, \mathbb{L}_3)$.

In addition, comparing the maximum values of $p_3^2$ and diff $(\mathbb{L}_2, \mathbb{L}_4)$ can be obtained

$$\max \text{diff}\,(\mathbb{L}_2, \mathbb{L}_2) = (V-2)U < h_3^2. \tag{E17}$$

Therefore, hole $p_3^2$ cannot be filled by the elements of diff $(\mathbb{L}_2, \mathbb{L}_4)$.

Next, it will be shown that hole $p_3^2$ can be filled with elements from diff $(\mathbb{L}_2, \mathbb{L}_4)$ only if $g = 1$. Assuming that $p_3^2$ can be filled with elements from diff $(\mathbb{L}_2, \mathbb{L}_4) = \{vU + 2L \mid v \in [2, 2U]\}$, there must be an integer $u$ that makes

$$U + V + UV + gV = vU + 2gV. \tag{E18}$$

Therefore

$$\frac{U+1-g}{1+v} = \frac{U}{V}. \tag{E19}$$

Because of $0 \leq v \leq V - 1$ and the coprime of $U$ and $V$, Equation (E18) holds under the condition $g = 1$. When $g > 1$, Equation (E18) does not hold, so hole $p_3^2$ cannot be filled by elements in diff $(\mathbb{L}_2, \mathbb{L}_4)$. Because of the primacy of $U$ and $V$, $U \geq 2$,

$$\left\lfloor \frac{U+1}{2} \right\rfloor \leq U - 1. \tag{E20}$$

Therefore, according to (E6), (E11), (E12), and (E20), $0 < g \leq \lfloor (U+1)/2 \rfloor$ can ensure that all holes of $\mathbb{P}_g$ and $\mathbb{P}_2^1$ and the first hole of $\mathbb{P}_3$ can be filled, that is, holes smaller than $\mathbb{P}_{e_1}$ in the range of $UV + U + V + L$ can be filled. Specifically, $\mathbb{P}_g \cap p_3^1$ can be filled by elements in diff $(\mathbb{L}_1, \mathbb{L}_3)$, and $\mathbb{P}_2^1$ can be filled by elements in diff $(\mathbb{L}_1, \mathbb{L}_2)$. It can therefore be further inferred that the first hole in the non-negative range of $\pm\mathbb{E}_1 \cup \pm\,\text{diff}\,(\mathbb{L}_1, \mathbb{L}_3)$ is located in $UV + gV + U + V$, that is, the number of continuous virtual elements in the set $\pm\mathbb{E}_1 \cup \pm\,\text{diff}\,(\mathbb{L}_1, \mathbb{L}_3)$ is $2(UV + gV + U + V) - 1$. It means that in the $0 < g \leq \lfloor (U+1)/2 \rfloor$ range, the greater the $g$ is, the higher the degree of freedom of the array is. Therefore, in order to translate the mutual-prime array to be able to obtain higher degrees of freedom, choose

$$g = \left\lfloor \frac{U+1}{2} \right\rfloor. \tag{E21}$$

Therefore, $L = \lfloor (U+1)/2 \rfloor V$ is the optimal translation distance. Based on the two cases discussed above, the following conclusions can be drawn: In order to maximize the number of continuous virtual elements of the translation mutual prime array, $L = \lfloor (U+1)/2 \rfloor V$ is the optimal translation distance, and the number of continuous virtual elements that can be generated is $2(UV + L + U + V) - 1$.

## REFERENCES


[1] Yan, H., Y. Wang, Y. Gong, Z. Zhang, and L. Wang, "Improved sparse symmetric arrays design for mixed near-field and far-field source localization," *IEEE Transactions on Aerospace and Electronic Systems*, Vol. 59, No. 6, 7486–7498, 2023.

[2] Gao, H., Y. Zhang, Y. Du, J. Cheng, and M. Chen, "Localization for mixed near-field and far-field sources under impulsive noise," *Journal of Systems Engineering and Electronics*, Vol. 35, No. 2, 302–315, 2023.

[3] Molaei, A. M., B. Zakeri, S. M. H. Andargoli, M. A. B. Abbasi, V. Fusco, and O. Yurduseven, "A comprehensive review of direction-of-arrival estimation and localization approaches in mixed-field sources scenario," *IEEE Access*, Vol. 12, 65 883–65 918, 2024.

[4] Schmidt, R., "Multiple emitter location and signal parameter estimation," *IEEE Transactions on Antennas and Propagation*, Vol. 34, No. 3, 276–280, 1986.

[5] Roy, R. and T. Kailath, "ESPRIT-estimation of signal parameters via rotational invariance techniques," *IEEE Transactions on Acoustics, Speech, and Signal Processing*, Vol. 37, No. 7, 984–995, 1989.

[6] Mei, F., H. Xu, W. Cui, B. Ba, and Y. Wang, "A transformed coprime array with reduced mutual coupling for DOA estimation of non-circular signals," *IEEE Access*, Vol. 9, 125 984–125 998, 2021.

[7] Ebrahimi, A. A., H. R. Abutalebi, and M. Karimi, "Localisation of mixed near-field and far-field sources using the largest aperture sparse linear array," *IET Signal Processing*, Vol. 12, No. 2, 155–162, 2018.

[8] Chen, G., X. Zeng, S. Jiao, A. Yu, and Q. Luo, "High accuracy near-field localization algorithm at low snr using fourth-order cumulant," *IEEE Communications Letters*, Vol. 24, No. 3, 553–557, 2019.

[9] Huang, S., B. Wang, Y. Zhao, and M. Luan, "Near-field RSS-based localization algorithms using reconfigurable intelligent surface," *IEEE Sensors Journal*, Vol. 22, No. 4, 3493–3505, 2022.

[10] Rinch, O., A. Elzanaty, and A. Alsharoa, "Enhancing near-field wireless localization with LiDAR-assisted RIS in multipath environments," *IEEE Wireless Communications Letters*, Vol. 12, No. 12, 2168–2172, 2023.

[11] Cao, X., A. Chen, H. Yin, and L. Chen, "A low-complexity near-field localization method based on electric field model," *IEEE Communications Letters*, Vol. 28, No. 2, 288–292, 2023.

[12] Zhang, X. and H. Zhang, "Hybrid reconfigurable intelligent surfaces-assisted near-field localization," *IEEE Communications Letters*, Vol. 27, No. 1, 135–139, 2022.

[13] He, J., L. Li, T. Shu, and T.-K. Truong, "Mixed near-field and far-field source localization based on exact spatial propagation geometry," *IEEE Transactions on Vehicular Technology*, Vol. 70, No. 4, 3540–3551, 2021.

[14] He, J., T. Shu, L. Li, and T.-K. Truong, "Mixed near-field and far-field localization and array calibration with partly calibrated arrays," *IEEE Transactions on Signal Processing*, Vol. 70, 2105–2118, 2022.

[15] Su, X., P. Hu, Z. Gong, Z. Liu, J. Shi, and X. Li, "Convolution neural networks for localization of near-field sources via symmetric double-nested array," *Wireless Communications and Mobile Computing*, Vol. 2021, No. 1, 9996780, 2021.

[16] Huang, Z., W. Wang, F. Dong, and D. Wang, "A one-snapshot localization algorithm for mixed far-field and near-field sources," *IEEE Communications Letters*, Vol. 24, No. 5, 1010–1014, 2020.

[17] Moffet, A., "Minimum-redundancy linear arrays," *IEEE Transactions on Antennas and Propagation*, Vol. 16, No. 2, 172–175, 1968.

[18] Pal, P. and P. P. Vaidyanathan, "Nested arrays: A novel approach to array processing with enhanced degrees of freedom," *IEEE Transactions on Signal Processing*, Vol. 58, No. 8, 4167–4181, 2010.

[19] Vaidyanathan, P. P. and P. Pal, "Sparse sensing with co-prime samplers and arrays," *IEEE Transactions on Signal Processing*, Vol. 59, No. 2, 573–586, 2010.

[20] Qin, S., Y. D. Zhang, and M. G. Amin, "Generalized coprime array configurations for direction-of-arrival estimation," *IEEE Transactions on Signal Processing*, Vol. 63, No. 6, 1377–1390, 2015.

[21] Wang, W., S. Ren, and Z. Chen, "Unified coprime array with multi-period subarrays for direction-of-arrival estimation," *Digital Signal Processing*, Vol. 74, 30–42, 2018.

[22] Yang, M., A. M. Haimovich, X. Yuan, L. Sun, and B. Chen, "A unified array geometry composed of multiple identical subarrays with hole-free difference coarrays for underdetermined DOA estimation," *IEEE Access*, Vol. 6, 14 238–14 254, 2018.

[23] Liu, C.-L. and P. P. Vaidyanathan, "Super nested arrays: Linear sparse arrays with reduced mutual coupling — Part I: Fundamentals," *IEEE Transactions on Signal Processing*, Vol. 64, No. 15, 3997–4012, 2016.

[24] Raza, A., W. Liu, and Q. Shen, "Thinned coprime array for second-order difference co-array generation with reduced mutual coupling," *IEEE Transactions on Signal Processing*, Vol. 67, No. 8, 2052–2065, 2019.

[25] Zheng, Z., W.-Q. Wang, Y. Kong, and Y. D. Zhang, "MISC array: A new sparse array design achieving increased degrees of freedom and reduced mutual coupling effect," *IEEE Transactions on Signal Processing*, Vol. 67, No. 7, 1728–1741, 2019.

[26] Zheng, Z., M. Fu, W.-Q. Wang, and H. C. So, "Symmetric displaced coprime array configurations for mixed near-and far-field source localization," *IEEE Transactions on Antennas and Propagation*, Vol. 69, No. 1, 465–477, 2020.

[27] Wu, X. and J. Yan, "A second-order statistics-based mixed sources localization method with symmetric sparse arrays," *IEEE Communications Letters*, Vol. 24, No. 8, 1695–1699, 2020.

[28] Wang, B., Y. Zhao, and J. Liu, "Mixed-order music algorithm for localization of far-field and near-field sources," *IEEE Signal Processing Letters*, Vol. 20, No. 4, 311–314, 2013.

[29] Zheng, Z., M. Fu, W.-Q. Wang, S. Zhang, and Y. Liao, "Localization of mixed near-field and far-field sources using symmetric double-nested arrays," *IEEE Transactions on Antennas and Propagation*, Vol. 67, No. 11, 7059–7070, 2019.

[30] Tian, Y., Q. Lian, and H. Xu, "Mixed near-field and far-field source localization utilizing symmetric nested array," *Digital Signal Processing*, Vol. 73, 16–23, 2018.

[31] Shen, J., T. Zhou, C. Xu, W. Zhang, and W. Du, "Localization for mixed far-field and near-field sources utilizing improved symmetric nested array," *Digital Signal Processing*, Vol. 107, 102879, 2020.

[32] Singh, P. R., Y. Wang, and P. Chargé, "A correction method for the near field approximated model based localization techniques," *Digital Signal Processing*, Vol. 67, 76–80, 2017.

[33] Zheng, Z., J. Sun, W.-Q. Wang, and H. Yang, "Classification and localization of mixed near-field and far-field sources using mixed-order statistics," *Signal Processing*, Vol. 143, 134–139, 2018.

[34] Pal, P. and P. P. Vaidyanathan, "Nested arrays: A novel approach to array processing with enhanced degrees of freedom," *IEEE Transactions on Signal Processing*, Vol. 58, No. 8, 4167–4181, 2010.